Journal of Power Sources 195 (2010) 6218–6224

Contents lists available at ScienceDirect

Journal of Power Sources

journal homepage: www.elsevier.com/locate/jpowsour

Modelling electrode material utilization in the trench model 3D-microbattery by finite element analysis

Vahur Zadin[a], Heiki Kasemägi[a], Alvo Aabloo[a], Daniel Brandell[b,*]

[a] Institute of Technology, Tartu University, Nooruse 1, 50411 Tartu, Estonia
[b] Department of Materials Chemistry, Uppsala University, The Ångström Laboratory, Box 538, SE-751 21 Uppsala, Sweden

ARTICLE INFO

Article history:
Received 16 October 2009
Received in revised form 17 February 2010
Accepted 19 February 2010
Available online 26 February 2010

Keywords:
Microbattery
Finite element method
Electronic conductivity
Electrode design

ABSTRACT

A mathematical model for ionic transport in 3D-microbattery (3D-MB) using finite element analysis is presented here, based on concentrated solution theory, ionic and atomic diffusion and the Butler–Volmer equation. The model is used to study electrochemical processes taking place in the electrodes and electrolyte of a 3D-MB in the trench architecture, with a 10 μm thick electrolyte layer separating 10 μm thick graphite anode and $LiCoO_2$ cathode plates. The effect of changing conductivity of the positive electrode and the electrode plate height is also studied. Qualitative and quantitative data describing battery performance in terms of concentration gradient development and discharge curves points out the range for the most favourable electronic conductivity values of the electrodes: the values should not differ by more than order of magnitude. Furthermore, it is shown that also with optimal electrode conductivity values for electrodes, the Li ion diffusion in the electrodes during discharge is limiting the performance of the battery due to inhomogeneous lithiation and delithiation. Changing electrode height can be used to fine tune surface area usage, but has a limited effect on the overall battery performance.

© 2010 Elsevier B.V. All rights reserved.

1. Introduction

Lack of suitable miniature portable power sources is currently an obstacle in the development of several technology areas, for example microelectromechanical devices (MEMS) and biomedical micro-machines. Here, the miniaturization of the microelectronics has far outpaced advances in small-scale power supplies [1]. In these devices, the limitations of conventional two-dimensional (2D) lithium ion batteries are apparent—on a small footprint area, it is not possible to achieve both sufficient power and energy density. This problem can be solved by developing batteries with three-dimensional (3D) architectures, where the electrode materials is stored on height. While a conventional 2D-battery has a sandwich architecture in a layer-by-layer configuration (Fig. 1), 3D microbatteries (3D-MB) have their components in a more complex spatial distribution. The increased surface area achieved by designing the battery in 3D can theoretically increase the power density within an order of magnitude or more. Fig. 2 presents some examples of proposed 3D-MB architectures: 3D-interdigitated (a), 3D-trench (b), 3D-concentric (c) and aperiodic (d) designs. It should be pointed out, however, that 3D-MB systems are still far from commercialization; so far only a few experimental 3D-MBs [2,3] and half cells have been made [4–6]. The "trench" design (Fig. 1b), developed by Notten et al. [7,8] is perhaps the most promising attempt. Here, an all-solid-state microbattery is approached by sputtering electrode and electrolyte materials on etched Si; the resulting samples show high rate-capability.

It is, however, unclear how the down-scaling and complex architecture of the 3D Li ion battery will affect the different electrochemical processes during battery operation. Here, mathematical modelling can make significant contributions. Different methods have long been used for modelling Li ion battery materials, ranging from electronic structure calculations and molecular dynamics to equivalent electronic network models.

Mathematical models covering the essential electrochemical processes for all critical components in conventional 2D Li ion batteries was pioneered by Newman et al. [9–12]. These models were one-dimensional, using porous electrode theory [13] to model the electrodes, and treated the electrodes as a uniform mix of active material, binder and electrolyte. The electrolyte was modelled by concentrated solution theory, while atomic transport in the active material particles was modelled by the radial diffusion equation (Fick's second law). The models have also been validated against experiment [14]. In recent work, Wang and Sastry [15] continued this approach using finite element analysis (FEA) to break down the electrode material mix in order to study the influence of size distribution of the active material particles.

A first attempt to model 3D-MB architectures were carried out by Hart et al. [16], who used FEA to calculate current densities and potentials for different electrode array configurations. They

* Corresponding author. Tel.: +46 184713747; fax: +46 18513548.
E-mail address: Daniel.Brandell@mkem.uu.se (D. Brandell).

0378-7753/$ – see front matter © 2010 Elsevier B.V. All rights reserved.
doi:10.1016/j.jpowsour.2010.02.056

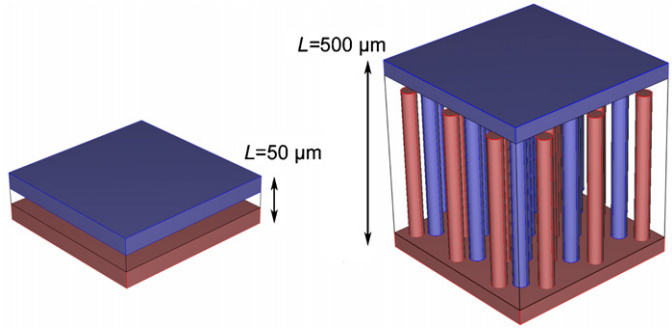

Fig. 1. Difference between a 2D and a 3D microbattery.

demonstrated that it is possible to reduce the difference in current density from 20% to 40% in a 3D-MB with interdigitated architecture (Fig. 2a) by changing the arrangement of the anode and cathode pillars. Moreover, it was possible to increase the homogeneity of the anode current, at the cost of decreasing it on cathode, by utilizing twice as many anodes as cathodes and surrounding every anode by six cathodes. This work showed the importance of taking the non-uniformity of the current density into account when modelling 3D-MBs, but did not analyse the electrochemistry in detail.

In the work presented here, we have extended Newman's approach [10] to 3D systems using FEA techniques. The aim has been to gain insights on different electrochemical aspects resulting from 3D-MB architectures, while at same time pointing out strategies for the optimization of the battery performance by varying its design.

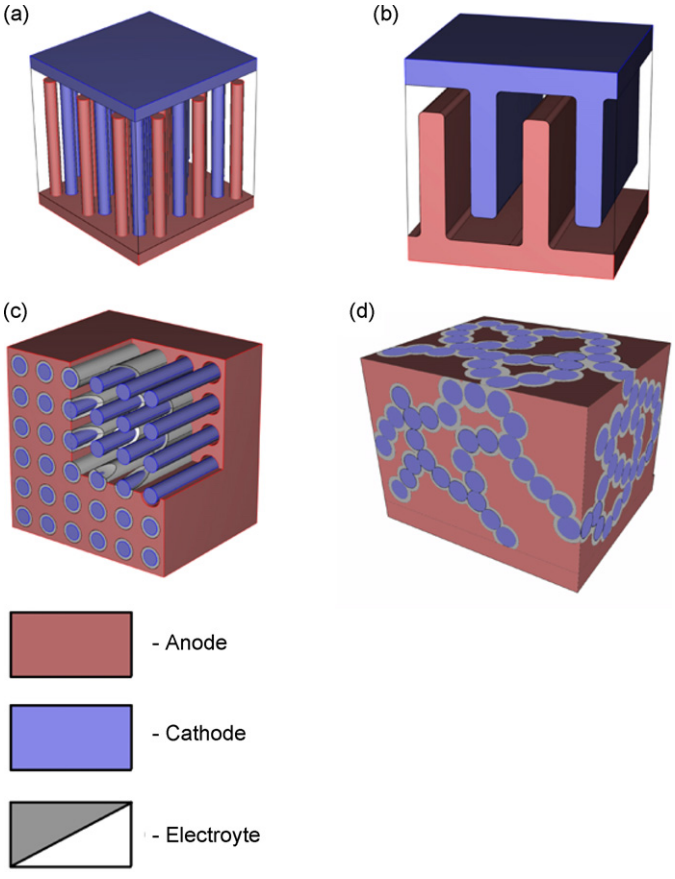

Fig. 2. Possible 3D-MB architectures: 3D-interdigitated (a), 3D-trench (b), 3D-concentric (c) and 3D-aperiodic (d).

2. Materials and methods

In this work, we have chosen to study conventional Li ion battery materials: $LiCoO_2$ as cathode, graphite as anode and an electrolyte consisting of 1.5 M solution of $LiPF_6$. These materials can be considered as a starting point; more realistic 3D-MB materials can be introduced in future studies. The electrochemical reactions in the electrodes are:

$$LiCoO_2 \underset{\text{discharging}}{\overset{\text{charging}}{\rightleftarrows}} Li_{1-x}CoO_2 + xLi^+ + xe^- \quad (0 \le x < 0.5) \tag{1}$$

$$C_6 + zLi^+ + ze^- \underset{\text{discharging}}{\overset{\text{charging}}{\rightleftarrows}} Li_zC_6 \quad (0 \le z \le 1) \tag{2}$$

We follow these processes in our model by the Li ion concentration. When the battery is fully discharged, the Li^+ concentration is at its maximum in the positive electrode ($LiCoO_2$), and at its minimum in the negative electrode (C_6). The situation is reversed when the battery is fully charged. Furthermore, the battery model consists of non-porous electrodes, comprising a solid mixture of active material and binder. As a result, Li ions are inserted into the electrolyte only at the geometrical electrode/electrolyte boundary areas. The constant discharge current was set to 18 $A\,m^{-2}$; other constants and parameters used are listed in Table 1.

2.1. Mathematical model

A detailed description of the mathematical model can be found in Newman's works [9–12]. Using this approach, we achieve a reasonable picture of the Helmholtz double layer in the electrolyte, which is necessary for studying the charging/discharging processes. Mass transfer in the active material can be considered to be controlled by diffusion, while processes taking place in the electrolyte can be modelled by concentrated solution theory with non-idealities neglected [17]. This mathematical model is based on the following assumptions:

1. Diffusion constants and conductivities are considered to be constant within their respective region in the battery (anode, cathode, electrolyte).
2. Active material particles and binder are assumed to form one solid non-porous electrode where atomic movement is described by diffusion.
3. Side reactions are neglected in the whole cell.
4. Electroneutrality is assumed in the electrolyte.
5. Volume changes in electrodes are neglected.
6. Charge transfer processes over the electrode–electrolyte interface (*i.e.*, the current density at the surface; J) are described by a Butler–Volmer kinetic expression [17]:

$$J = i_0 \left[\exp\left(F\alpha_a \frac{\eta}{RT} \right) - \exp\left(-F\alpha_c \frac{\eta}{RT} \right) \right] \tag{3}$$

where i_0 is exchange current density, α_a is anodic and α_c is cathodic transfer coefficients; $\alpha_a = \alpha_c = 0.5$. η is the surface overpotential, calculated from:

$$\eta = \varphi_1 - \varphi_2 - U_{oc} \tag{4}$$

where U_{oc} is the open circuit potential, and φ_1 and φ_2 are potentials in the electrode and electrolyte, respectively. The open circuit potential in the electrodes is fitted from experimental data using piecewise polynomials [18].

Since the anodic and cathodic transfer coefficients are set equal, *i.e.*, $\alpha_a = \alpha_c = \alpha = 0.5$, the concentration dependent exchange current density can be calculated as [17]:

$$i_0 = F(k_a)^{\alpha_c}(k_c)^{\alpha_a}(c_{s\max} - c_s)^{\alpha_c} c_s^{\alpha_a} c^{\alpha_a} \tag{5}$$

Table 1
Parameters used in the simulations.

Symbol	Quantity	Value	Ref.
D^*_{Li}	Diffusion constant of Li^+ in the electrode	2×10^{-13} m^2 s^{-1}	[20]
D_{Li}	Diffusion constant of Li^+ in the electrolyte	2×10^{-11} m^2 s^{-1}	[21]
D_{PF6}	Diffusion constant of PF_6^- in the electrolyte	3×10^{-11} m^2 s^{-1}	[21]
σ_1	Electronic conductivity of positive electrode	0.01 S m^{-1}	
σ_2	Ionic conductivity of electrolyte	1×10^{-3} S m^{-1}	
σ_3	Electronic conductivity of negative electrode	1 S m^{-1}	
c_0	Initial salt concentration in electrolyte	1500 mol m^{-3}	
c^+_{s0}	Initial Li^+ concentration in positive electrode	24.4 mol dm^{-3}	
c^-_{s0}	Initial Li^+ concentration in negative electrode	27.2 mol dm^{-3}	
c^+_{smax}	Maximum Li^+ concentration in positive electrode	51.6 mol dm^{-3}	
c^-_{smax}	Maximum Li^+ concentration in negative electrode	28.2 mol dm^{-3}	
J_0	Charging/discharging current	18 A m^{-2}	
t_0	Transference number	0.5	
α	Transfer coefficient	0.5	

where c is the concentration in electrolyte, c_s is the concentration in electrode, c_{smax} is the maximum concentration in electrode, and α_a is anodic and α_c is cathodic transfer coefficients, $\alpha_a = \alpha_c$. Changes of c^α were only a few percent during the simulations, which validates the approximation of a constant concentration. The system under study has a low constant current, resulting in a uniform concentration profile in electrolyte similar to the initial values. c in Eq. (5) can therefore be considered constant, c_0 (1.5 M), which is a necessary approximation since the complex electrolyte geometry is sensitive to non-linearities arising from the Butler–Volmer and exchange current density equations. k_a and k_c are rate constants for the anodic and cathodic directions of the reactions, respectively; the model parameter $k^0 = (k_a)^{\alpha_c}(k_c)^{\alpha_a}$ is estimated from Ref. [15] to maintain current balance in the simulations.

7. Constant transference numbers are assumed at all times throughout the electrolyte ($t_0 = 0.5$).

In contrast to a porous electrode model, Li^+ insertion is described by the boundary conditions, not as reaction rate term, resulting in a slightly modified mathematical description. For example, the potential in the electrolyte (φ_2), calculated according to concentrated solution theory, is described by the following equations [17]:

$$\nabla \cdot (\sigma_2 \nabla \phi_2 - \kappa_D \nabla \ln(c)) = 0 \tag{6}$$

$$\vec{n} \cdot (\sigma_2 \nabla \phi_2 - \kappa_D \nabla \ln(c)) = -J \tag{7}$$

where c, σ and n are concentration, conductivity and normal unit vector, respectively. The current density J at the boundary is calculated by the Butler–Volmer equation (Eq. (3)), and κ_D is calculated from:

$$\sigma_2 = \frac{2RT}{F}(1 - t_0)\kappa \tag{8}$$

where σ_2 is the ionic conductivity of electrolyte.

The potentials in the electrodes (φ_1) are calculated according to Ohm's law [17]:

$$\nabla \cdot (\sigma_i \nabla \phi_1) = 0, \quad i = 1,3 \tag{9}$$

$$\vec{n} \cdot \nabla \phi_1 = \frac{J}{\sigma_i} \tag{10}$$

Eq. (10) is used as a boundary condition on the electrode–electrolyte boundary. J is again calculated by Butler–Volmer equation (Eq. (3)). The boundary condition at the positive electrode's current collector is:

$$\vec{n} \cdot \nabla \phi_1 = \frac{-J_0}{\sigma_1} \tag{11}$$

where J_0 is charging or discharging current; the potential is set to zero on negative electrode's current collector. Using constant current density over the whole surface of the electrode boundary is only causing minor deviations to our simulation results, since the difference between maximum and minimum potential values on the electrode surface is below 1%.

The mass transport in the electrolyte is described by concentrated solution theory [17]:

$$\frac{\partial c}{\partial t} = \nabla (D \nabla c) \tag{12}$$

At the electrode–electrolyte boundary, the absence of an anionic diffusive flux has to be taken into account. The anion diffusion is therefore balanced by migration, leading to the boundary condition [17]:

$$\vec{n} \cdot \nabla c = \frac{-J(1 - t_0)}{FD} \tag{13}$$

where $(1 - t_0)$ is accounting for migration. The rest of the migration is described by Eqs. (6)–(7). In Eqs. (12)–(13):

$$D = \frac{2(D_{Li} D_{PF6})}{(D_{Li} + D_{PF6})} \tag{14}$$

is the diffusion coefficient of the $LiPF_6$ electrolyte. The boundary condition (Eq. (13)) is applied to all boundaries between electrode and electrolyte. Periodic boundary condition for concentration is applied to the rest of boundaries in electrolyte.

The material balance in the electrodes is described by [17]:

$$\frac{\partial c_s}{\partial t} = \nabla (D^*_{Li} \nabla c_s) \tag{15}$$

$$\vec{n} \cdot \nabla c_s = \frac{J}{F D^*_{Li}} \tag{16}$$

where D^*_{Li} is the diffusion coefficient of lithium in the electrode material. Again, boundary condition (Eq. (16)) is applied to the electrode–electrolyte boundary.

2.2. Geometrical models

The geometrical model used in these studies is the *trench model*; see Fig. 2b. This is currently one of the more practically realizable models to work with [7,8]. The basic geometry used in the simulations, which has been systematically altered in the studies, comprises electrolyte filled trenches of width 10 μm, separating electrode plates of 100 μm height and a thickness of 10 μm. The system is infinite in two dimensions through periodic boundary conditions. The plates in the model consist fully of active materials, with flat current collectors on top. This differs from the

experimental systems [7,8], where the electrodes are deposited on pre-fabricated 3D current collector plates, but resembles on the other hand earlier 3D-MB FEA models [15].

2.3. Simulations

In order to achieve maximum capacity, material usage and peak current of a 3D-MB – equivalent to optimizing its power density – the surface area of the electrode must be utilized as efficiently as possible. This is achieved automatically in a 2D-battery, where the electrodes are coplanar, making the current distribution homogeneous. A 3D-battery, however, has a complex electrode shape and must be carefully designed to achieve uniform electrochemical activity on the electrode surface. This is more or less impossible to investigate systematically with experimental methods, but computer modelling can give significant insights. Here, the electrochemically active surface area has been evaluated from the Li^+ ion concentration gradient. When the concentration gradient is homogeneous on the entire electrode/electrolyte interface, the battery architecture can be considered optimal in terms of electrochemical activity.

The current distribution in a 3D-MB – which controls the concentration gradient – depends on diffusion coefficients, processes in the solid–electrolyte interface (SEI) layer, temperature, side reactions, electrode shape, *etc*. Two of the most important parameters are the electronic conductivity in the electrodes and the dimensions of the electrodes, which together control the current flow through the battery geometry. In the simulations performed within this study, we investigate the effects of altering the geometrical plate height and the value of the electronic conductivity of the positive electrode, respectively, during the full 3D-MB discharge process. First, simulations were carried out for the 100 μm plates with conductivities 1, 0.75, 0.5, 0.25, 0.1, 0.05 and 0.01 S m^{-1} on the positive electrode. The lower value is more realistic, while the higher could be achieved by adding electronically conductive material to the cathode slurry. The conductivity of negative electrode (graphite) was fixed at 1 S m^{-1}. Thereafter, the discharge cycle was simulated at fixed conductivity values of 0.01 and 1 S m^{-1} in the positive and negative electrodes, respectively, while the height of the electrode plates were changed from 100 to 75, 50, 25 or 10 μm. The voltage was cut-off when the discontinuity appeared in the current, which made the voltage drop significantly. This generally appeared at ~3.5 V. This discontinuity at the end of the discharge was caused by inability of the battery to deliver the current required by the boundary conditions. All other parameters were fixed according to Table 1.

2.4. Mesh density and solver settings

Eqs. (3)–(16) have been solved using the COMSOL Multiphysics 3.5 and COMSOL Script 1.3 software. For the electrode conductivity studies, it was possible to use the same mesh in all simulations, while a new mesh was generated for every new geometry in the electrode height studies. To ensure accurate results, the element sizes were decreased stepwise until the solutions for c_i and φ_i (i = 1,2) in Eqs. (6)–(16) converged. Quadratic second order finite elements were used in the electrolyte, a triangular mesh in the bulk of the electrode material, while a boundary layer mesh was used for the electrodes, resulting in a dense quadratic element mesh on the electrode–electrolyte boundary. The resulting meshes consisted of approximately 13,000 elements in the conductivity studies and between ~1500 and 13,000 elements in the electrode height studies. A generalized-α integrator in conjunction with PARDISO solver was used to solve time dependent matrix equation. The integrator had 0.01 relative and 0.001 absolute tolerance.

3. Results and discussion

3.1. Influence of electrode conductivity

The electrochemical activity on the electrode/electrolyte interface has been evaluated by the development of the ionic concentration profiles and the corresponding discharge curves. The applied discharge current (J_0) over the entire current collector area was 18 A m^{-2}.

Simulated battery discharge curves for different electronic conductivity values for the positive electrode are presented in Fig. 3. The curves show good agreement with experimental data for 2D graphite/$LiCoO_2$ systems [19], and display the typical behaviour of a fast voltage drop, subsequent stabilization and a voltage drop at the end of the discharge cycle when the battery is completely discharged. The discharge curves for positive electrode conductivity values between 0.25 and 1 S m^{-1} are almost completely overlapping, suggesting that the electrochemical processes are very similar for these cathodes. It can therefore be concluded that it is inefficient to try to increase the conductivity of the positive electrode beyond 0.25 S m^{-1}, as long as the conductivity of the negative electrode is kept at 1 S m^{-1}.

At constant current, the power output of the battery is directly proportional to the voltage ($P = U \times I$). It is thus possible to estimate how the change in conductivity affects the relative performance of the battery. Significant changes in performance appear when the conductivity of the positive electrode drops below 0.1 S m^{-1}; and the performance is lowest at 0.01 S m^{-1}. For 0.01 S m^{-1}, the battery power output at the beginning of simulation is ~3% lower than for 1 S m^{-1}, and ~9% lower by the end of the discharge process.

This effect can be understood by studying the electrochemical processes in the electrodes in detail. Fig. 4 displays the concentration profile development in the electrodes when the conductivity of positive electrodes is 1 S m^{-1} (equal to the negative electrode). The delithiation and lithiation of the electrodes starts directly from the plate tips. As the discharge proceeds, fast depletion and accumulation of Li ions continue in these regions of the electrodes. This is due to the inhomogeneous current density distribution in the system, caused by the electrode tip being considerably smaller than the corresponding surface of the opposite plate. Ions exiting the tip therefore spread over a larger surface on the opposite electrode, and the current density is therefore concentrated to the tips—a direct effect of the 3D design. Consequently, although the negative and positive electrodes are delithiated and lithiated at the same pace, the higher local reaction rates at the plate tips will limit the current through the battery since the tips of the electrodes are

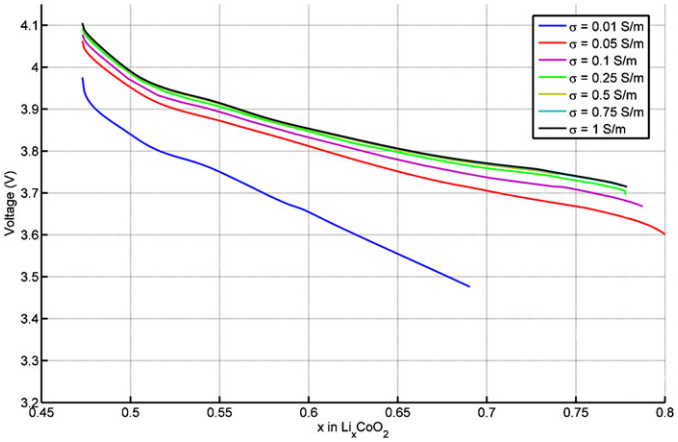

Fig. 3. Discharge curves for different conductivity values for the positive electrode. Discharge curves representing σ = 0.5, 0.75 and 1 S m^{-1} are overlapping.

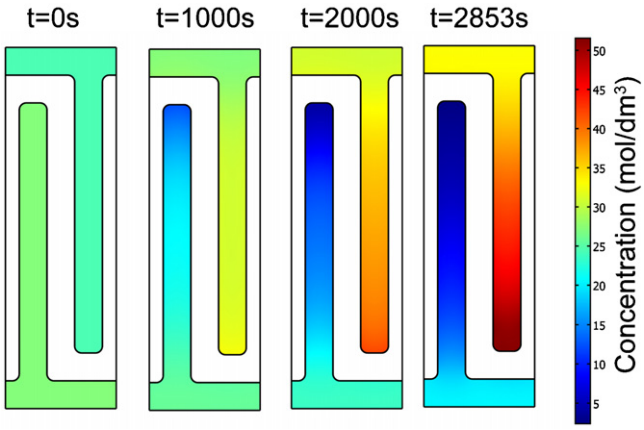

Fig. 4. Concentration profile development in the 3D-MB electrodes. Top electrode: $LiCoO_2$, positive; bottom electrode: LiC_6, negative. Conductivities of the electrodes are both 1 S m^{-1}.

depleted faster. The current then has to find a different route, which ends the electrochemical processes prematurely. Therefore, only approximately to 80% of the theoretical capacity is achieved (see Fig. 3).

The concentration gradient development in the electrolyte – directly proportional to the ionic current density – is presented in Fig. 5 for simulations with equal electrode conductivity (1 S m^{-1}). At 100 s after the beginning of the discharge, the concentration gradient distribution in the electrolyte is more or less equal, indicating that the electrochemical activity is uniform at the surfaces. After 500 s, however, the electrochemical activity is clearly concentrated to the tip of the negative electrode and the bottom part of the positive electrode. The electrochemical activity at the positive electrode tip is approximately 2–3 times smaller than the negative tip. As the discharge proceeds (at 1000 and 1500 s), the electrochemical activity oscillate back and forth at the negative electrode tip and the side of the plates, indicating that the tip is periodically getting depleted of lithium ions. At the same time, the activity is maintained rather uniform at the positive electrode. These results are consistent with Fig. 4 at $t = 1000$ s, where a more uniform distribution of electrochemical activity can be observed at the positive electrode surface, equivalent to a more homogeneous lithiation of the entire plate. At the same time, the negative electrode plate tip is slightly more delithiated than the rest of the electrode. At $t = 1500$ s (Fig. 5), the electrochemical activity at the tip of the positive electrode increases, parallel with increasing activity on the bottom of the negative electrode. This process continues at $t = 2000$ s and $t = 2500$ s, where the electrochemical activity at the positive electrode surpasses that of the negative.

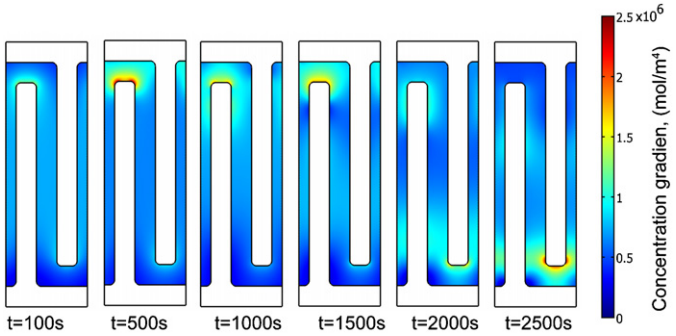

Fig. 5. Concentration gradient development in the electrolyte. The electrodes have equal electronic conductivity (1 S m^{-1}).

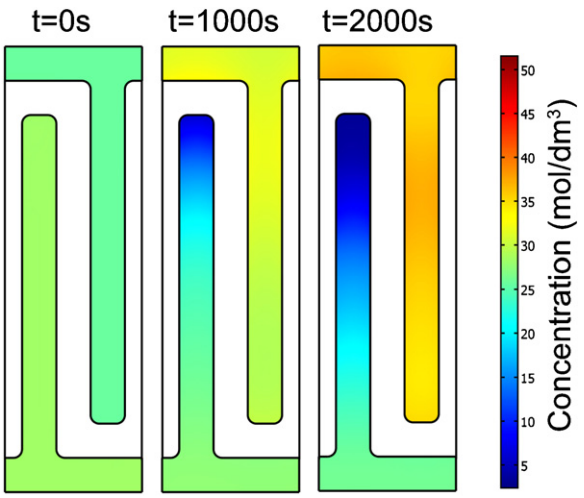

Fig. 6. Concentration profile development in the 3D-MB electrodes. Top electrode: $LiCoO_2$, positive; bottom electrode: LiC_6, negative. Conductivities of the electrodes are 1 S m^{-1} for LiC_6 and 0.01 S m^{-1} for $LiCoO_2$.

It could be assumed that the equality of the electrode conductivity values should result in equal electrochemical activity on both electrodes due to symmetry. The observed non-uniformities in Figs. 4 and 5 are caused by several factors. The most significant reason is probably that the surface overpotential η (Eq. (4)) in the Butler–Volmer equation (Eq. (3)) becomes larger on the negative electrode due to different open circuit potentials for the electrode materials, causing a non-uniform potential drop in the electrolyte.

Interestingly, at $t = 2500$ s when the positive electrode tip is fully lithiated, the electrochemical activity is still very high in this region. According to the Butler–Volmer equation, the current moving through this part should approach zero. The electrochemical activity can instead be explained from the bottom part of the negative electrode, where x is ≈0.8 in Li_xCoO_2. This allows the build-up of a high local overpotential (Eq. (4)), and lithium therefore diffuse from the highly lithiated area at the tip of the positive electrode towards less concentrated areas at the bottom of the same plate, enabling the continuation of the charging process at the tip. Since the lithiation apparently is preferred at the $LiCoO_2$ electrode tip, the charging becomes dependent on the solid-state diffusion in the electrode.

It is obvious from Figs. 4 and 5 that even a very favourable combination of conductivity values results in inhomogeneous electrochemical activity in the 3D-MB, mainly at the tips of the electrode plates. This problem is introduced by the geometry itself: the surface area difference between the tip and the opposite bottom electrode leads to a specific current density distribution, which, in turn, leads to an inhomogeneous discharge. This problem could perhaps be tackled using different 3D-MB architectures, like 3D-concentric and 3D-aperiodic designs, or increasing diffusion coefficient of Li—for example using porous electrodes.

When the conductivity of the positive electrode is decreased to 0.01 S m^{-1} (the negative electrode still having 1 S m^{-1}), the situation changes; see Fig. 6. As the discharge begins, the delithiation of the negative electrode again starts from the tip of the negative electrode. In contrast to Fig. 4, where the conductivities are equal, the charging of the positive electrode does not begin at the electrode tip, but rather uniformly over the entire plate. The large conductivity difference gives rise to the non-uniformities in the Li^+ depletion of negative electrode—the electrical current in the 3D-MB is now to a higher extent going through the negative electrode plate due to its lower resistance. Therefore, the electrode tip is depleted fast in order to maintain a constant current, which accord-

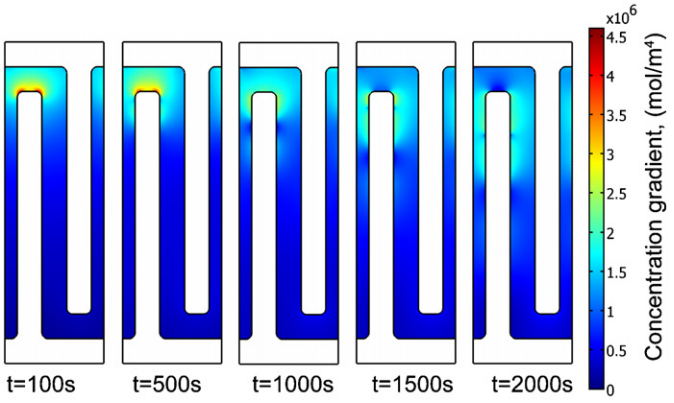

Fig. 7. Concentration gradient development in the electrolyte. The conductivity of the positive electrode is 0.01 S m^{-1}, while the conductivity of the negative electrode is 1 S m^{-1}.

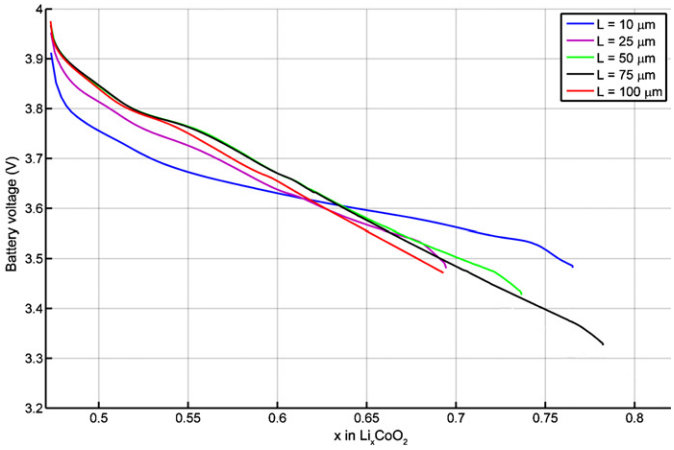

Fig. 9. Discharge curves for 3D-MBs with different electrode plate heights.

ing to Eq. (5) makes the exchange current density approach zero and subsequently decrease the electrical current moving through the electrode surface in accordance with the Butler–Volmer equation (Eq. (3)). As a result, the extensive depletion of active material at the plate tip limits the performance of the entire battery, which can also be observed in Fig. 3. The discharge process finishes at $x \approx 0.68$ in Li_xCoO_2 when the cut-off voltage is reached.

The time development of the activity in the electrolyte when the conductivity of the positive electrode is 0.01 S m^{-1} is presented in Fig. 7. The most active part is the tip of the negative electrode plate and, unlike when the electrodes have equal conductivity, the electrochemical activity does not alternate between the electrodes. The activity is considerably high at the electrode tip up to 1000 s after the start of the discharge process, thereafter the reaction rate decreases and eventually drops to zero as the electrode is depleted. Meanwhile, the sides of the negative electrode plate become increasingly electrochemically active. At 2000 s, approximately 40% of the negative electrode plate surface is active. This suggests that if the electrode materials have large conductivity differences, the efficiency can be increased by shortening the plate height, since this may optimize electrode material usage.

3.2. Influence of electrode height

The concentration gradient development for plates with 50 μm height is presented in Fig. 8, which can be compared to the 100 μm electrodes in Fig. 7. The results for plate heights of 25 or 75 μm resemble this example. At the beginning of the discharge cycle, the concentration gradient development for 50 μm electrodes is similar to 100 μm electrodes. The delithiation of the negative electrode again begins at the negative electrode tip and, after this area is depleted, continues at the electrode plate sides. However, by the end of the simulation (t = 1500 s), almost the whole surface area of the electrode is electrochemically active.

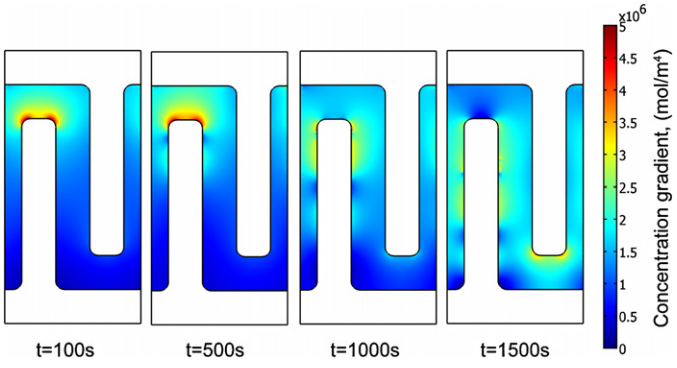

Fig. 8. Concentration gradient development in the electrolyte for a 3D-MB with electrode plates of 50 μm height. The conductivity of the positive electrode is 0.01 S m^{-1}, while the conductivity of the negative electrode is 1 S m^{-1}.

The discharge curves of the simulated batteries with different electrode plate heights are summarized in Fig. 9. All curves begin with a typical fast drop in cell voltage at the beginning of the discharge cycle, and then go through a continuous voltage drop at steady rate until the cut-off voltage is reached. The voltage drop at the end of the discharge cycle for plate height 10 μm occurs at higher voltage values, indicating that the depletion of the cell for this particular geometry is more complete than for the other configurations at this particular discharge current. The plate height 10 μm results in a final $x \approx 0.77$ in Li_xCoO_2. For all other geometries, the final voltage drop appears when the cell voltage is approximately 3.32–3.48 V, *i.e.*, below the general cut-off voltage. This is an effect of the non-uniform Li^+ depletion at the negative electrode (visible in Fig. 8) which leads to a premature end of the delithiation. As a result, the positive electrode is within the range $Li_{0.69}CoO_2$–$Li_{0.78}CoO_2$ at the end of discharge for plate heights above 10 μm.

The discharge curves for electrode heights between 25 and 100 μm are almost identical, indicating similarities in the electrochemically active regions and in the discharge processes. When the plate height is 10 μm, on the other hand, the characteristics are much more different—it has the sharpest voltage drop at the beginning, but the slowest voltage drop during the rest of the discharge process. For such a small electrode plate height, the geometry is approaching a flat 2D configuration, and the typical inhomogeneous ionic transport processes of a 3D-MB are less pronounced. Most of the electrode surface is active already at the beginning of the simulation, which is the reason for the fast initial voltage drop (see Fig. 9). For the taller plates, the large areas with low electrochemical activity make the voltage drop at the beginning of discharge less distinct. Using 10 μm plates, the capacity of the active material is thus closer to its theoretical value, but on the other hand, less material can be stored using this configuration.

To illustrate the total effect of the electrode plate height to the battery capacity, the battery voltage dependence from discharge time is presented in Fig. 10. By normalizing the difference in electrode volume, the plate height L = (10, 25, 50, 75, 100) μm corresponds to an increase in electrode volume with a factor 1, 1.3, 1.8, 2.5 and 2.8, respectively. This correlates well with the increasing discharge time seen in Fig. 10, where electrodes with plate lengths L = (10, 25, 50, 75, 100) μm are discharged during t = (1000, 1300, 1700, 2450, 2100) s, respectively. The only significant exception is

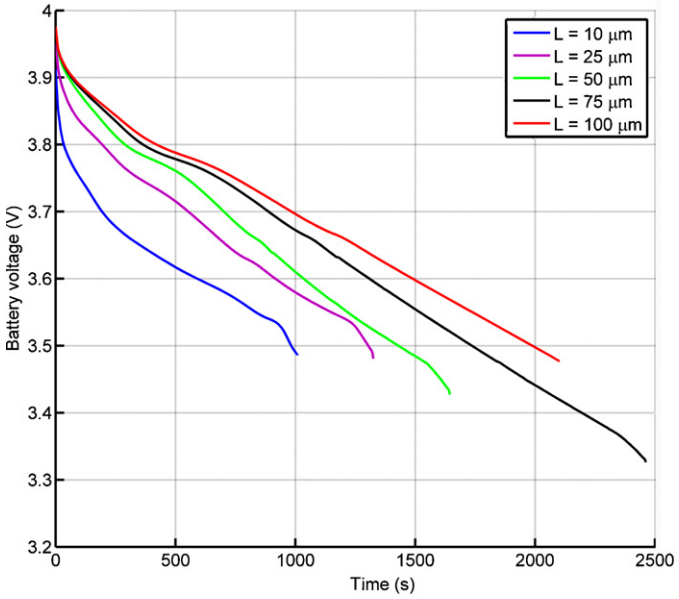

Fig. 10. Battery voltage development for electrodes with different heights. A constant discharge current of 18 A m^{-2} was used.

the 100 μm electrode. Considering Fig. 9, this is probably caused by the lower lithiation rate at the positive electrode.

4. Conclusions

In this work, FEA has been used to study the influence of material properties (electronic conductivity) and geometrical design (plate height) for the trench model of a 3D-MB. The simulation comprise the entire battery, using concentrated solution theory for the electrolyte, Fick's diffusion law for the solid electrodes, and a Butler–Volmer approach to model transport kinetics over the electrode/electrolyte boundary.

When altering the electronic conductivity of the positive electrode, it can be concluded that the most favourable positive electrode conductivity values range from 0.25 to 1 S m^{-1} for a negative electrode conductivity of 1 S m^{-1}. These values results in up to 9% larger power output as compared to positive electrodes with $\sigma = 0.01$ S m^{-1}. Furthermore, the amount of Li in Li_xCoO_2 is considerably higher at the end of discharge when the conductivities are similar. For unequal electrode conductivities, the electrochemical activity on the surfaces of the electrodes can be fine tuned by monitoring the height of the electrode plates. Shorter plates give more efficient discharge. However, shorter plates give a loss in capacity, since the amount of electrode material is decreased; the benefits from a 3D geometry are lost.

The simulations show that it is impossible to achieve a homogeneous lithiation/delithiation of the electrodes with this trench 3D-MB design. The electrode plate tips are lithiated/delithiated much faster than other parts of the electrodes, and therefore a limiting factor for the battery performance. This result should also have bearing for the 3D-interdigitated architecture, since it origins from the difference in surface area between the electrode tip and the opposing electrode, which gives a non-uniform current density. However, this problem can be overcome using porous electrodes, which increase the Li ion diffusion in these parts of the battery.

Currently, several simplifications are included in the mathematical model. The exchange current density approximation limits the maximum current, and the diffusion coefficients and electronic conductivities are kept constant within the electrode and electrolyte, while they should be dependent on ionic concentration. The model should include these phenomena in future work. More realistic materials and geometries should also be modelled. Last, there is a need for experimental data on 3D-MBs in order to validate the model.

Acknowledgements

This work has been financed by the EU-FP7 project *SUPERLION*. VZ is indebted to the Kristian Jaak foundation, Ångpanneföreningens forskningsstiftelse, and Estonian Science Foundation grant #6765.

References

[1] J.W. Long, B. Dunn, D.R. Rolison, H.S. White, Chem. Rev. 104 (2004) 4463–4492.
[2] D. Golodnitsky, M. Nathan, V. Yufit, E. Strauss, K. Freedman, L. Burstein, A. Gladkich, E. Peled, Solid State Ionics 177 (2006) 2811–2819.
[3] H. Min, B.Y. Park, L. Taherabadi, C. Wang, Y. Yeh, R. Zaouk, M.J. Madou, B. Dunn, J. Power Sources 178 (2008) 795–800.
[4] G.T. Teixidor, R.B. Zaouk, B.Y. Park, M.J. Madou, J. Power Sources 183 (2008) 730–740.
[5] E. Perre, L. Nyholm, T. Gustafsson, P. Taberna, P. Simon, K. Edström, Electrochem. Commun. 10 (2008) 1467–1470.
[6] P.L. Taberna, S. Mitra, P. Poizot, P. Simon, J. Tarascon, Nature Mater. 5 (2006) 567–573.
[7] P.H.L. Notten, F. Roozeboom, R.A.H. Niessen, L. Baggetto, Adv. Mater. 19 (2007).
[8] L. Baggetto, R.A.H. Niessen, F. Roozeboom, P.H.L. Notten, Adv. Funct. Mater. 18 (2008) 1057.
[9] M. Doyle, T.F. Fuller, J. Newman, J. Electrochem. Soc. 140 (1993) 1526–1533.
[10] T.F. Fuller, M. Doyle, J. Newman, J. Electrochem. Soc. 141 (1994) 1–10.
[11] P.M. Gomadam, J.W. Weidner, R.A. Dougal, R.E. White, J. Power Sources 110 (2002) 267–284.
[12] J. Newman, K.E. Thomas, H. Hafezi, D.R. Wheeler, J. Power Sources 119–121 (2003) 838–843.
[13] J.S. Newman, C.W. Tobias, J. Electrochem. Soc. 109 (1962) 1183–1191.
[14] M. Doyle, J. Newman, A.S. Gozdz, C.N. Schmutz, J. Tarascon, J. Electrochem. Soc. 143 (1996) 1890–1903.
[15] C. Wang, A.M. Sastry, J. Electrochem. Soc. 154 (2007) 1035–1047.
[16] R.W. Hart, H.S. White, B. Dunn, D.R. Rolison, Electrochem. Commun. 5 (2003) 120–123.
[17] J. Newman, in: W.V. Schalkwijk, B. Scrosati (Eds.), Advances in Lithium-ion Batteries, Springer, 2002.
[18] A.T. Stamps, S. Santhanagopalan, E.P. Gatzke, J. Electrochem. Soc. 154 (2007) P20–P27.
[19] Q. Zhang, Q. Guo, R.E. White, J. Power Sources 165 (2007) 427–435.
[20] L. Sebastian, J. Gopalakrishnan, J. Mater. Chem. 13 (2003) 433–441.
[21] D. Danilov, P. Notten, Electrochim. Acta 53 (2008) 5569–5578.